


## Article

# Sr, S, and O Isotope Compositions of Evaporites in the Lanping–Simao Basin, China

Lijian Shen <sup>1</sup>, Licheng Wang <sup>2,\*</sup>, Chenglin Liu <sup>1</sup> and Yanjun Zhao <sup>1</sup>

<sup>1</sup> MNR Key laboratory of Metallogeny and Mineral Assessment, Institute of Minerals Resources, Chinese Academy of Geological Sciences, Beijing 100037, China; shenlijian1019@126.com (L.S.); liuchengl@263.net (C.L.); zhaoyanjun266@163.com (Y.Z.)

<sup>2</sup> CAS Center for Excellence in Tibetan Plateau Earth Sciences, Key Laboratory of Continental Collision and Plateau Uplift, Institute of Tibetan Plateau Research, Chinese Academy of Sciences, Beijing 100101, China

\* Correspondence: lichengwang@itpcas.ac.cn

**Abstract:** Evaporites are widely distributed within continental “red beds” in the Lanping–Simao Basin, west Yunnan, China. Sr (Strontium), S (Sulfur), and O (Oxygen) isotope compositions have been measured on 54 sulfate or/and sulfate-bearing samples collected from Lanping, Nuodeng, Jinggu, Mengyejing, Baozang throughout the Lanping–Simao Basin. The  $^{87}\text{Sr}/^{86}\text{Sr}$  ratios of all samples (0.708081 to 0.710049) are higher than those of contemporaneous seawater, indicating a significant continental contribution to the drainage basin. Sulfates in the Lanping Basin have higher  $^{87}\text{Sr}/^{86}\text{Sr}$  ratios (0.709406 to 0.710049) than those (0.708081 to 0.709548) in the Simao Basin. Nevertheless, the  $\delta^{34}\text{S}$  values of gypsums (13.4‰ to 17.6‰) in Lanping and Baozang fall within the range of Cretaceous seawater. Gypsums from a single section in Baozang have trends of decreasing  $\delta^{34}\text{S}$  values and increasing  $^{87}\text{Sr}/^{86}\text{Sr}$  ratios from base to top, indicating continental input played an increasingly significant role with the evaporation of brines. High  $\delta^{34}\text{S}$  values (20.5‰ to 20.7‰) of celestites in Lanping are probably caused by bacterial sulfate reduction (BSR) process in which  $^{34}\text{S}$  were enriched in residual sulfates and/or recycling of Triassic evaporites. The reduced  $\delta^{34}\text{S}$  values of gypsums (9.5‰ to 10.4‰) in Nuodeng could have been caused by oxidation of sulfides weathered from Jinding Pb–Zn deposit. The complex O isotope compositions indicate that sulfates in the Lanping–Simao Basin had undergone sulfate reduction, re-oxidation, reservoir effects, etc. In conclusion, the formation of continental evaporites was likely derived from seawater due to marine transgression during the Cretaceous period. Meanwhile, non-marine inflows have contributed to the basin significantly.



**Citation:** Shen, L.; Wang, L.; Liu, C.; Zhao, Y. Sr, S, and O Isotope Compositions of Evaporites in the Lanping–Simao Basin, China. *Minerals* **2021**, *11*, 96. <https://doi.org/10.3390/min11020096>

Academic Editor:

Krzysztof Bukowski

Received: 23 November 2020

Accepted: 15 January 2021

Published: 20 January 2021

**Publisher’s Note:** MDPI stays neutral with regard to jurisdictional claims in published maps and institutional affiliations.



**Copyright:** © 2021 by the authors. Licensee MDPI, Basel, Switzerland. This article is an open access article distributed under the terms and conditions of the Creative Commons Attribution (CC BY) license (<https://creativecommons.org/licenses/by/4.0/>).

**Keywords:** evaporites; the Lanping–Simao Basin; continental setting; sulfates; Sr; S; O isotopes

## 1. Introduction

The Lanping–Simao Basin hosts the only ancient potash deposit ever found in China [1], and a great quantity of metallic mineral resources which have a close relationship with evaporites, especially sulfates [2–5]. Consequently, the origin of those evaporites has attracted tremendous attention during the last decades [6–13]. The basin evolved from a remnant marine and marine-continental basin during the Triassic Period, through a continental depression basin during the Jurassic–Cretaceous Period, to a pull-apart continental basin during the Cenozoic Period [2]. Evaporites were primarily formed within the Triassic and Cretaceous periods during the evolution of the basin. The metallic-associated gypsums in the Sanhedong Formation, upper Triassic, was marine origin [2,14], whereas the sources of evaporites within Cretaceous continental “red beds” remain a subject of debate. The Br (bromide) geochemistry of rock salts in the Mengyejing potash deposit indicates a major seawater contribution [11,15]. On the contrary, Li et al. (2015) [16] suggested a major continental origin based on geochemical evidence of the Mengyejing potash deposit. Qu et al. (1998) [10] proposed that evaporites in the Lanping–Simao Basin formed during

Cretaceous to Tertiary were typical continental origin based on sedimentary facies. However, Wang et al. (2014a) [12] suggested that the Cretaceous gypsums from the Lanping Basin were mainly derived from seawater based on S isotope compositions. A series of saline lakes formed during the Late Cretaceous from north to south of the Lanping–Simao Basin wherein a certain amount of evaporites (mainly sulfates and chlorides) were deposited [17]. Consequently, a comprehensive study of those evaporites is needed to refine our understanding of their origin.

Sr, S, and O isotope studies are useful for recording origin, deposition, and paleoclimate, etc. [18]. The S, O, and Sr isotopic compositions of marine evaporites are well constrained through the Phanerozoic [19–23]. In comparison to marine evaporites, these isotopic compositions of continental evaporites are more complex depending on local geology and hydrology within the drainage basin [24]. In this paper, we present S, Sr, and O isotopic compositions of continental lacustrine evaporites, which occurred in Mesozoic–Cenozoic “red beds” in the Lanping–Simao Basin, west Yunnan, China [10]. The objectives of this study are to (1) determine the origin of parent brines in which evaporites precipitated; (2) interpret paleo-environmental changes during deposition of evaporites.

## 2. Geological Setting

The Lanping–Simao Basin is located in western Yunnan, China, stretching along the NW–SE direction. Tectonically, the Lanping–Simao Basin is a part of the Simao Block which is separated from the South China Block by the Jinshajiang–Ailaoshan sutures to the east, and from the Baoshan and Sibumasu blocks by the Jinghong and Changning–Menglian sutures to the west [25]. The basin is divided into two parts, namely the Lanping Basin to the north and the Simao Basin to the south (Figure 1).

The Lanping–Simao Basin developed on the paleo-Tethys basement since the collision between Simao and South China blocks in the Late Triassic and evolved from a remnant marine and marine-continental basin of the Triassic [2] into a continental rift basin of the Jurassic–Cretaceous period [10]. The Jurassic–Early Cretaceous sedimentary deposits consist of a thick sequence of continental red beds. These red beds are unconformably overlain by the Late Cretaceous continental evaporites and clastic deposits [26]. Lacustrine siltstones and mudstones with evaporites sequences are widespread within the Mengyejing Formation in the Simao Basin and Yunlong Formation in the Lanping Basin (Figure 2). These two formations were previously thought to have been formed during Paleocene based on Ostracoda and Charophyta assemblages [10]. However, updated evidence of SHRIMP zircon U–Pb dating of tuff beds within the Mengyejing Formation supported a mid-Cretaceous age, 100–110 Ma [27]. Chen (2017) [28] postulated that the Yunlong Formation was formed during the late Cretaceous based on the maximum depositional age evidenced by detrital zircon U–Pb dating. Although the correlation regarding the formation age between the Mengyejing formation and the Yunlong formation still remains a subject of debate, we believe these two formations are equivalent and deposited during the Late Cretaceous. The major evaporite minerals in the Mengyejing and Yunlong formations are composed of gypsum and halite, with a small amount of sylvite and carnallite [10].

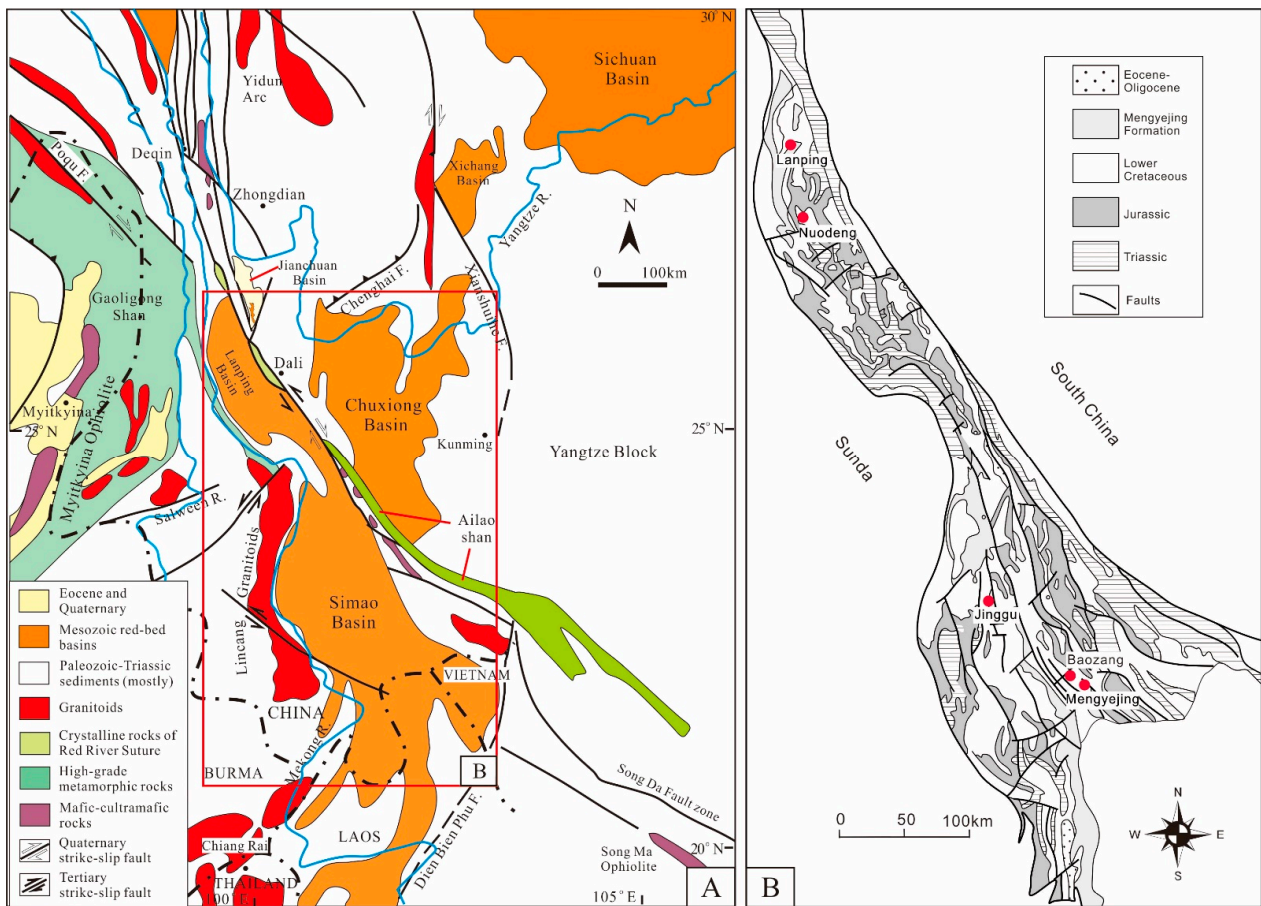


**Figure 1.** (A) Schematic map of major tectonic features of western Yunnan (after [29]); (B) schematic geological map of Lanping–Simao Basin and sampling locations (marked by red dots) (after [27]).

Age	Lanping Basin	Thickness/m	Lithology	Simao Basin
Paleogene	E <sub>2b</sub> Baoxiangsi Fm	800	Conglomerate, sandstone, sandy-mudstone	Mengla Fm
	E <sub>2g</sub> Guolang Fm	500-800	Sandstone, siltstone interlayered with mudstone	Denghei Fm
Cretaceous	K <sub>2</sub> -E <sub>0</sub> ? Yunlong Fm	266-800	Mudstone, siltstone, intercalated with evaporites	Mengyejing Fm
	K <sub>1h</sub> Hutousi Fm	28-213	Sandstone	Pashahe Fm
	K <sub>1n</sub> Nanxing Fm	514-1960	Sandstone, siltstone	Mangang Fm
	K <sub>1j</sub> Jingxing Fm	412-1465	Silty-mudstone, sandstone	Jingxing Fm
Jurassic	J <sub>3b</sub> Bazhulu Fm	83-1324	Mudstone intercalated with fine-grained sandstone	Bazhulu Fm
	J <sub>2h</sub> Huakaizuo Fm	118-1343	Sandstone sandy-mudstone, intercalated with carbonate	Hepingxiang Fm
	J <sub>1y</sub> Yangjiang Fm	64-2038	Sandy-mudstone	Zhangkezhai Fm
Triassic	T <sub>3m</sub> Maichujing Fm	~1000	Sandy-mudstone, sandstone interlayered with mudstone	Manghuaihe Fm

**Figure 2.** The synthesized stratigraphic column of the Mesozoic-Tertiary sedimentation (modified from [29]).

### 3. Materials and Methods

A variety of samples, including layered and veined gypsums, rock salts were collected from Lanping, Nuodeng, Jinggu, Baozang, and Mengyejing from the north to the south of the Lanping–Simao Basin. Sulfate samples (mostly gypsums) stemmed from outcrops located in Lanping, Nuodeng, Jinggu, and Baozang. Rock salt samples were sampled from the underground mine lane of the Mengyejing potash deposit (Figure 3).

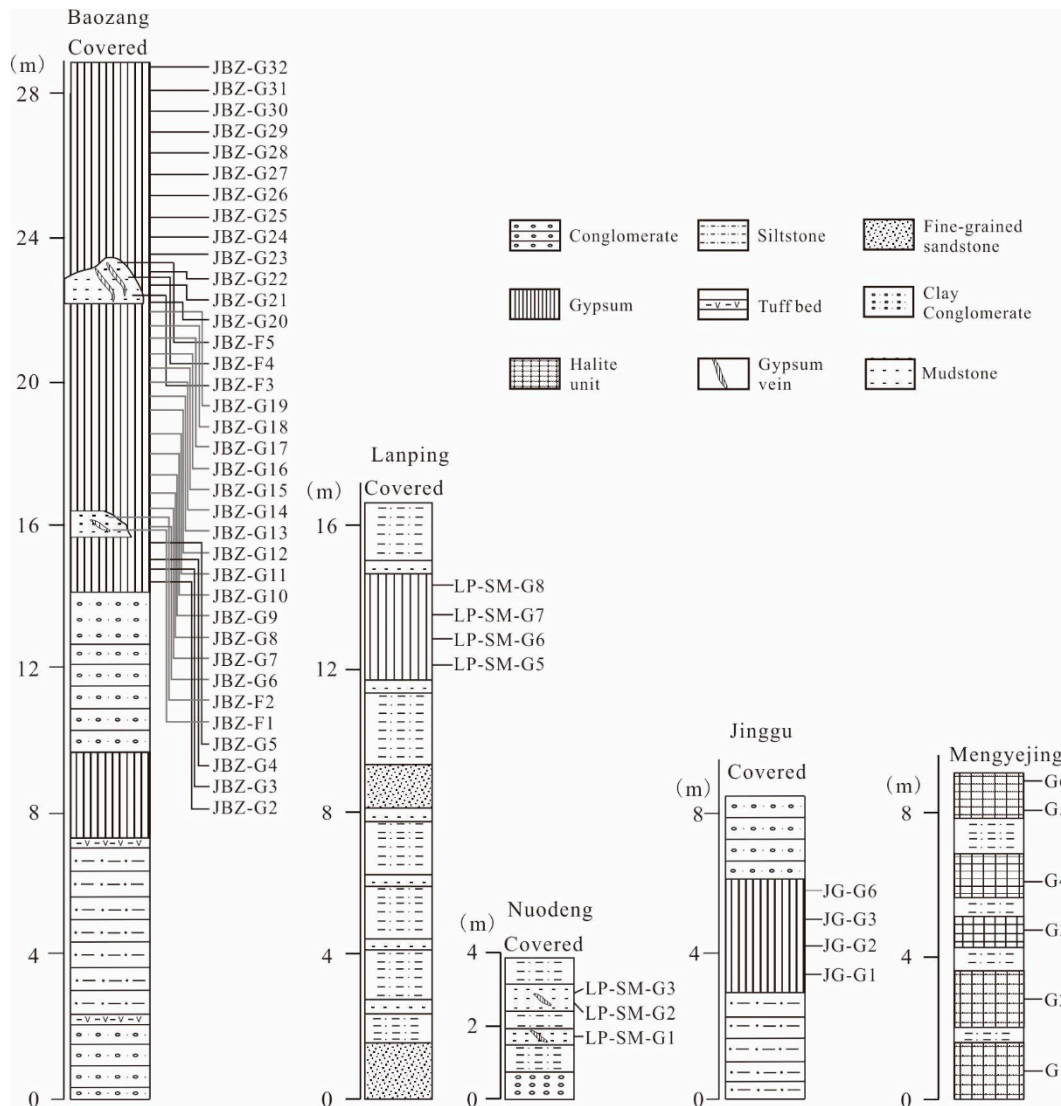


**Figure 3.** Sampling sections/sites from Baozang, Lanping, Nuodeng, Jinggu, and Mengyejing.

Four samples were collected from gypsum laminae in Lanping; three samples were collected from vein-shaped gypsums in Nuodeng; four samples were collected from gypsum laminae in Jinggu; 37 samples were collected in Baozang, including 32 laminated gypsum samples and five veined gypsum samples. Six rock salt samples were collected from the underground mine lane of the Mengyejing potash deposit.

In order to select samples with sufficient sulfate for analyzing S isotope composition, all samples were tested by X-ray diffraction (XRD) analysis. To eliminate the effect of sulfides, all examples were examined under binoculars.

All samples collected from the Lanping–Simao Basin were cut, polished, and thinned using an oil system. The thin sections were examined using a polarizing microscope.

The SEM analysis was carried out at the Key Laboratory of Deep-Earth Dynamics, Institute of Geology using the FEI Nova NanoSEM 450. The back scattered electron (BSE) images were taken under operating voltage of 15–20 KV and working distance of 13.5 mm.

Sr isotope analyses of all samples were performed at the State Key Laboratory of Isotope Geochemistry, Guangzhou Institute of Geochemistry, Chinese Academy of Sciences. Powdered gypsum samples (~5 to 10 mg) were dissolved with 4M HNO<sub>3</sub> after washing with milli-Q water. Five to 10 g of rock salt samples were washed with milli-Q water to eliminate chloride salts and accumulated sulfates and subsequently dissolved with 4M HNO<sub>3</sub>. Sr was extracted from the samples using a Sr-specresin. The detailed procedure about Sr separation is given by [30]. Samples were analyzed in a Neptune Plus multi-collector (MC) ICP-MS. The <sup>87</sup>Sr/<sup>86</sup>Sr ratios were corrected for mass discrimination using <sup>87</sup>Sr/<sup>86</sup>Sr ratio = 0.1194. NBS 987 standard yields <sup>87</sup>Sr/<sup>86</sup>Sr values of 0.71022(30) and 0.71030 (7) for MC-ICP-MS spectrometers. Uncertainties in the <sup>87</sup>Sr/<sup>86</sup>Sr are quoted in 1σ.

Oxygen isotopic composition of sulfates were performed at the State Key Laboratory of Lithosphere Evolution, Institute of Geology and Geophysics, Chinese Academy of Sciences. Sulfates were dissolved and reacted with BaCl<sub>2</sub> solutions. The precipitated BaSO<sub>4</sub> was washed and dried. Solid barite samples were weighed into a silver capsule and introduced into a graphite furnace where BaSO<sub>4</sub> is converted to CO gas at 1400 °C in helium gas using a thermal combustion elemental analyzer (TCEA). Oxygen isotope ratios were measured by a continuous flow isotope ratio monitoring mass spectrometry system using a Flash HT 2000 high temperature pyrolysis furnace coupled with a Finnigan ConFlo IV open split interface to a Thermo Scientific DELTA V Advantage mass spectrometer. Measurements were calibrated using the two-point linear normalization method based on international sulfate standards NBS 127 (+8.6‰, VSMOW), IAEA SO-5 (+12.13‰, VSMOW). Repeated measurements of international standards (four measurements per standard per run) yield reproducibility of better than 0.2‰ (1σ) for oxygen isotope measurements.

For the S isotope measurement, the sulfate was combusted at 980°C in a Flash Element Analyzer and the resulting sulfur dioxide (SO<sub>2</sub>) was measured with continuous flow GS-IRMS (Thermo, Delta V Plus) at the Beijing Research Institute of Uranium Geology. δ<sup>34</sup>S values are reported vs. the Canyon Diablo Troilite (CDT), and the error was determined using the standard deviation of the standard (GBW-04414 and GBW-04415) at the beginning and the end of each run (<0.5‰).

The detailed procedure for ICP-MS trace element analysis is given in [31], and the two-sigma error for the <sup>87</sup>Rb/<sup>86</sup>Sr ratio was estimated at ±2.6%.

## 4. Results

### 4.1. Characteristics of Evaporite Minerals

In Lanping, the gypsum section is interbedded with the underlying and overlying mudstones (Figure 3) with relatively sharp contact boundary. The mudstones show massive structure. Gypsum aggregates are usually present as two forms, i.e., gypsum laminae with fine-grained crystals (alabaster) and selenite macrocrystallines. The common millimetric gypsum laminae show slightly wavy features (Figure 4A) and are seen as alabaster on planar direction (Figure 4B). Selenite crystals are sporadically interbedded or embedded with gypsum laminae. The boundary between selenite and gypsum laminae are sharp (Figure 4A). The gypsum laminae are composed of microcrystalline gypsum. The microcrystalline gypsums display a variety of textures ranging from xenotopic to idiotopic. The crystals are present primarily as xenotopic ameboid gypsums with minor embedded euhedral crystals (Figure 5A). The gypsum crystals showed no orientation and variation in sorting. The sizes of the microcrystalline gypsums are equant and not varied along with the changes of the laminae. The scanning electron microscopy (SEM) analysis showing that euhedral pyrite (Figure 5B) and celestite are present within gypsum laminae (Figure 5C).



**Figure 4.** Characteristics of evaporites in the Lanping–Simao Basin. (A) Bedded gypsum layers in Lanping; (B) gypsum alabasters, Lanping; (C) gypsum veins within clastic rocks, Nuodeng; (D) satin spar gypsums, Nuodeng; (E) gypsum laminae, Jinggu; (F) millimetric gypsum layers (light color) interbedded with calcareous layer (dark grey color), Jinggu; (G) gypsum sections in Baozang; (H) gypsum laminae coexisting with selenite crystals, Baozang; (I) gypsum veins within mudstone breccias, Baozang; (J) satin spar gypsums intercalated with clastic rocks; (K) bedded rock salts in underground mine lane from Mengyejing; (L) organic matters within gypsum layers, adjacent to Mengyejing.

In Nuodeng, fractures are developed within mottled (reddish-brown and greenish-grey) clastic rocks, and filled by nearly pure gypsum veins (Figure 4C). These veins consist of fibers from 1 to 10 cm long. The gypsum fibers are curved and show perpendicular or oblique orientation to the wall rocks (Figure 4D). The elongated gypsum crystals within veins are curved and aligned with minor distorted relative short gypsum crystals (Figure 5D). The clastic rocks are unconsolidated and showing stratified structure with no cross-bedding detected. Some parts of the clastic rocks contain clayey breccias (Figure 4C,D).

In Jinghong, gypsum laminae are normally organized in millimetric to centimetric beds (Figure 4E), alternating with calcareous clastic layers. The stratified gypsum laminae and intercalated calcareous clastic layers are plane-parallel. The lamination is clearly differentiated by white and gray thin layers (Figure 4F). In thin section the white laminae were seen as small gypsum nodules displaying ameboid texture (Figure 5E). Anhydrite relics with jagged edges surrounded by granular gypsums are detected within the thin layer gypsums, showing dehydration and rehydration processes (Figure 5F).

In Baozang, gypsum laminae are mingled with mudstones and/or siltstones (Figure 4G). The bedding structure is distinct based on color banding (Figure 5G). Some parts of the gypsum laminae are replaced by nodular selenite (Figure 4H). In nodular selenite, swallowtail-

shaped gypsum crystals (Figure 5H) and corroded anhydrite crystals (Figure 5I) are detected, suggesting a similar dehydration–rehydration process to that in Jinghong. Interstratified and vertical fractures (Figure 4H) are filled with satin spar gypsums (veined gypsums). In addition to those veined gypsums within laminae fractures, some wired gypsum veins are present in clayey or silty breccias (Figure 4I). The gypsum fibers are perpendicular or oblique to the surface of the wall rocks. Relatively long gypsum laths occur within clastic rocks, showing slightly curved features (Figure 4J). Microphotographs of gypsum laths show herringbone pattern (Figure 5J).

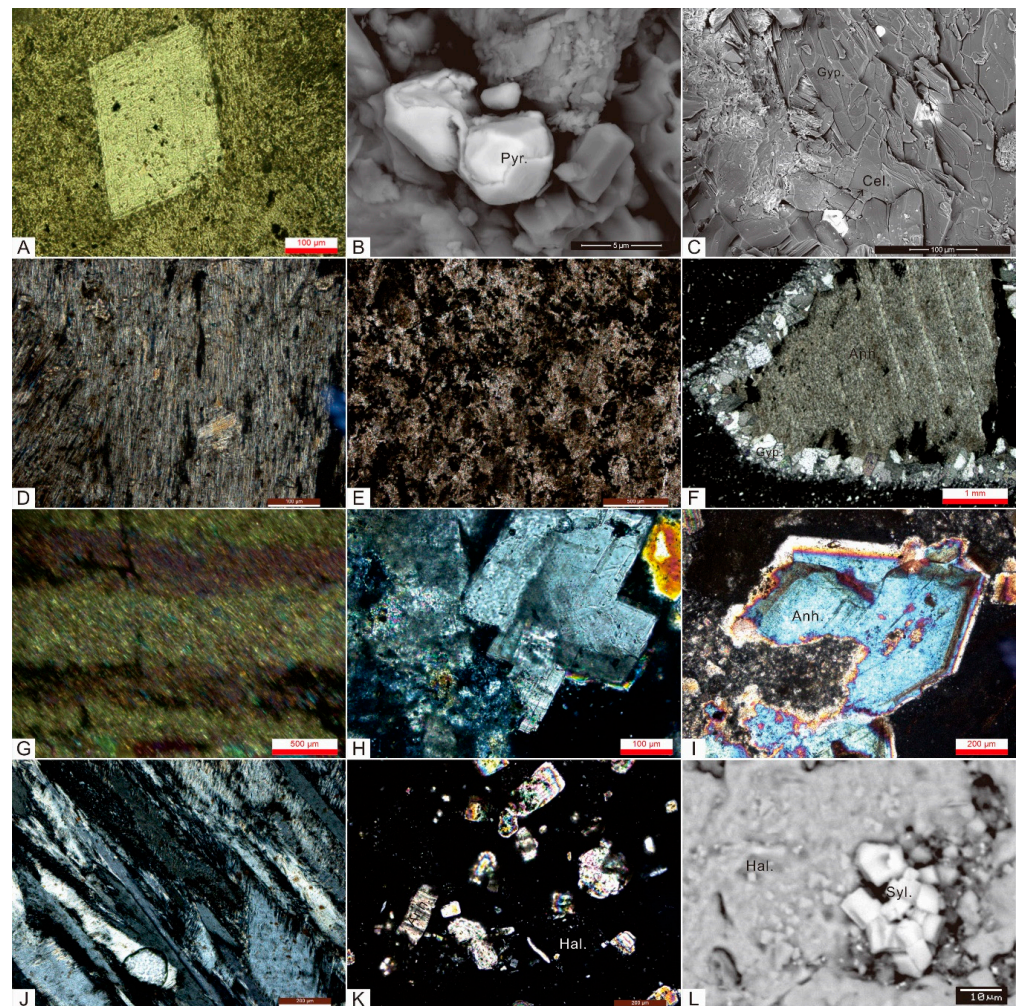


**Figure 5.** Photomicrographs of the evaporite minerals within the Mengyejing Formation. (A) ameoboid and rhomboidal gypsums, Lanping, cross-polarized light (CPL); (B) pyrite crystals within gypsums, Lanping, scanning electron microscopy (SEM) image; (C) euhedral celestite crystal within gypsums, Lanping, SEM image; (D) aligned gypsum fibers, Nuodeng, CPL; (E) ameoboid gypsums, Jinggu, CPL; (F) anhydrite relics with surrounding gypsum grains, Jinggu, CPL; (G) alternating microcrystalline gypsum layers and calcareous or/and silty layers, Baozang; (H) euhedral selenite crystals, Baozang, CPL; (I) anhydrite relics with corroded features coexisting with microcrystalline gypsums, Baozang, CPL; (J) aligned gypsum laths with herringbone features, Baozang, CPL; (K) euhedral anhydrite crystals within halites, Mengyejing, CPL; (L) euhedral sylvite crystals on the surface of halites, Mengyejing, SEM image.

In Mengyejing, the underground potash deposit consists of rhythmically alternating clastic rocks and evaporites. The clastic rocks are composed of unconsolidated mudstones and siltstones. The chloride salts, namely, halite sylvite or carnallite are crosscutting or cementing most mudstones and siltstones. The layers of the orebody are dipping nearly

vertically due to tectonic deformation (Figure 4K). The rock salt samples are primarily composed of halite, with trace amounts of euhedral anhydrites (Figure 5K) and sylvites (Figure 5L).

#### 4.2. XRD Results

The mineral components are measured using XRD analyses. The result shows that gypsum samples in Lanping consist of approximately 90% gypsum and 10% calcite, with a trace amount of quartz. Two celestite-bearing samples in Lanping contain approximately 40% and 10% celestite, 55% and 90% calcite, respectively. Samples in Nuodeng consist exclusively of gypsum, except for sample LP-SM-G3 with a small amount of quartz and albite. The major mineral of samples in Jinggu are gypsum (90% to 100%), and subordinate amounts of calcite, dolomite, and magnesite (Table 1). Halite is the most abundant mineral in samples from Mengyejing, with NaCl content ranging from 65% to 100%. Anhydrites and gypsums are present as a minor constituent. Some samples contain a certain amount of carbonates and potash minerals (Table 1). Samples from Baozang are composed of nearly pure gypsums, with a trace amount of bassanite, carbonates, and quartz (Table 1).

**Table 1.** Semi-quantitative X-ray diffraction (XRD) analyses of samples from different locations.

Location	Sample ID	Age	Formation	Compositions, Based on XRD Analyses	Lithology
Lanping	LP-SM-G5	late Cretaceous?	Yunlong	90% gypsum, 10% calcite, and trace quartz	Gypsum laminae
Lanping	LP-SM-G6	late Cretaceous?	Yunlong	55% calcite, 40% celestite, 5% quartz	Gypsum laminae
Lanping	LP-SM-G7	late Cretaceous?	Yunlong	90% gypsum, 10% calcite, and trace quartz	Gypsum laminae
Lanping	LP-SM-G8	late Cretaceous?	Yunlong	90% calcite, 10% celestite	Gypsum laminae
Nuodeng	LP-SM-G1	late Cretaceous?	Yunlong	100% gypsum	Gypsum veins
Nuodeng	LP-SM-G2	late Cretaceous?	Yunlong	100% gypsum	Gypsum veins
Nuodeng	LP-SM-G3	late Cretaceous?	Yunlong	93% gypsum, 3% quartz, and trace albite	Gypsum veins
Jinggu	JG-G1	late Cretaceous	Mengyejing	100% gypsum	Gypsum laminae
Jinggu	JG-G2	late Cretaceous	Mengyejing	95% gypsum, 5% calcite	Gypsum laminae
Jinggu	JG-G3	late Cretaceous	Mengyejing	90% gypsum, 5% calcite, 5% magnesite	Gypsum laminae
Jinggu	JG-G6	late Cretaceous	Mengyejing	90% gypsum, 20% dolomite,	Gypsum laminae
Mengyejing	G1	late Cretaceous	Mengyejing	nearly 100% halite, trace gypsum	
Mengyejing	G2	late Cretaceous	Mengyejing	nearly 100% halite, trace gypsum	Layered rock salts
Mengyejing	G3	late Cretaceous	Mengyejing	95% halite, 5% anhydrite	Layered rock salts
Mengyejing	G4	late Cretaceous	Mengyejing	70% halite, 10% anhydrite, 10% quartz	Layered rock salts
Mengyejing	G5	late Cretaceous	Mengyejing	65% halite, 15% quartz, 10% anhydrite, 10% dolomite	Layered rock salts
Mengyejing	G6	late Cretaceous	Mengyejing	85% halite, 15% sylvite, trace anhydrite	Layered rock salts
Baozang	JBZ-F1	late Cretaceous	Mengyejing	100% gypsum	Gypsum veins
Baozang	JBZ-F2	late Cretaceous	Mengyejing	100% gypsum	Gypsum veins
Baozang	JBZ-F3	late Cretaceous	Mengyejing	100% gypsum	Gypsum veins
Baozang	JBZ-F4	late Cretaceous	Mengyejing	85% gypsum, 15% bassanite	Gypsum veins
Baozang	JBZ-F5	late Cretaceous	Mengyejing	100% gypsum	Gypsum veins
Baozang	JBZ-G02	late Cretaceous	Mengyejing	98% gypsum, trace quartz	Gypsum laminae
Baozang	JBZ-G03	late Cretaceous	Mengyejing	100% gypsum	Gypsum laminae
Baozang	JBZ-G04	late Cretaceous	Mengyejing	100% gypsum	Gypsum laminae
Baozang	JBZ-G05	late Cretaceous	Mengyejing	100% gypsum	Gypsum laminae
Baozang	JBZ-G06	late Cretaceous	Mengyejing	nearly 100% gypsum, trace quartz	Gypsum laminae



Table 1. Cont.

Location	Sample ID	Age	Formation	Compositions, Based on XRD Analyses	Lithology
Baozang	JBZ-G07	late Cretaceous	Mengyejing	nearly 100% gypsum, trace bassanite	Gypsum laminae
Baozang	JBZ-G08	late Cretaceous	Mengyejing	nearly 100% gypsum, trace quartz	Gypsum laminae
Baozang	JBZ-G09	late Cretaceous	Mengyejing	100% gypsum	Gypsum laminae
Baozang	JBZ-G10	late Cretaceous	Mengyejing	100% gypsum	Gypsum laminae
Baozang	JBZ-G11	late Cretaceous	Mengyejing	100% gypsum	Gypsum laminae
Baozang	JBZ-G12	late Cretaceous	Mengyejing	100% gypsum	Gypsum laminae
Baozang	JBZ-G13	late Cretaceous	Mengyejing	100% gypsum	Gypsum laminae
Baozang	JBZ-G14	late Cretaceous	Mengyejing	100% gypsum	Gypsum laminae
Baozang	JBZ-G15	late Cretaceous	Mengyejing	100% gypsum	Gypsum laminae
Baozang	JBZ-G16	late Cretaceous	Mengyejing	100% gypsum	Gypsum laminae
Baozang	JBZ-G17	late Cretaceous	Mengyejing	nearly 100% gypsum, trace quartz	Gypsum laminae
Baozang	JBZ-G18	late Cretaceous	Mengyejing	100% gypsum	Gypsum laminae
Baozang	JBZ-G19	late Cretaceous	Mengyejing	100% gypsum	Gypsum laminae
Baozang	JBZ-G20	late Cretaceous	Mengyejing	100% gypsum	Gypsum laminae
Baozang	JBZ-G21	late Cretaceous	Mengyejing	100% gypsum	Gypsum laminae
Baozang	JBZ-G22	late Cretaceous	Mengyejing	100% gypsum	Gypsum laminae
Baozang	JBZ-G23	late Cretaceous	Mengyejing	95% gypsum, 5% calcite	Gypsum laminae
Baozang	JBZ-G24	late Cretaceous	Mengyejing	95% gypsum, 5% quartz	Gypsum laminae
Baozang	JBZ-G25	late Cretaceous	Mengyejing	100% gypsum	Gypsum laminae
Baozang	JBZ-G26	late Cretaceous	Mengyejing	100% gypsum	Gypsum laminae
Baozang	JBZ-G27	late Cretaceous	Mengyejing	98% gypsum, trace quartz	Gypsum laminae
Baozang	JBZ-G28	late Cretaceous	Mengyejing	95% gypsum, 5% dolomite	Gypsum laminae
Baozang	JBZ-G29	late Cretaceous	Mengyejing	98% gypsum, trace calcite	Gypsum laminae
Baozang	JBZ-G30	late Cretaceous	Mengyejing	nearly 100% gypsum, trace quartz	Gypsum laminae
Baozang	JBZ-G31	late Cretaceous	Mengyejing	100% gypsum	Gypsum laminae
Baozang	JBZ-G32	late Cretaceous	Mengyejing	100% gypsum	Gypsum laminae
Baozang	JBZ-G33	late Cretaceous	Mengyejing	100% gypsum	Gypsum laminae

#### 4.3. Sr, S and O Isotopes

The  $^{87}\text{Sr}/^{86}\text{Sr}$  ratios of all samples in the Lanping Basin range from 0.709406 to 0.710049, which are much higher than those of the Late Cretaceous seawater [22]. The celestite-bearing samples have slightly higher  $^{87}\text{Sr}/^{86}\text{Sr}$  ratios compared with the gypsum samples (Table 2). The  $^{87}\text{Sr}/^{86}\text{Sr}$  ratios of the gypsum samples in the Simao basin range from 0.708081 to 0.709548 (Jinggu: 0.708081 to 0.708792, Baozang: 0.708114 to 0.709548). There is considerable overlap between the  $^{87}\text{Sr}/^{86}\text{Sr}$  ratios of Baozang and Jinggu. The  $^{87}\text{Sr}/^{86}\text{Sr}$  ratios of the rock salt samples range from 0.709717 to 0.710071, which are higher than those of gypsum samples in Jinggu and Baozang (Figure 6A).

**Table 2.** Sr, S, and O isotope compositions of evaporite samples within the Lanping–Simao Basin.

Location	Sample ID	$\delta^{18}\text{O}\text{‰}$	$\delta^{34}\text{S}_{\text{V-CDT}}$	$^{87}\text{Sr}/^{86}\text{Sr}$	Rb (ppm)	Sr (ppm)	Rb/Sr
Lanping	LP-SM-G5	21.6	14.5	$0.709622 \pm 0.000005$	1.34	3572	0.0003751
	LP-SM-G6	18.4	20.5	$0.710049 \pm 0.000007$	0.678	>5000	<0.0001356
	LP-SM-G7	23.1	17.6	$0.709845 \pm 0.000008$	0.483	4699	0.0001028
	LP-SM-G8	17	20.7	$0.710039 \pm 0.000005$	2.05	>5000	<0.00041
Nuodeng	LP-SM-G1	6.8	10.2	$0.709406 \pm 0.000013$	2.59	192	0.0134896
	LP-SM-G2	-	9.5	$0.709438 \pm 0.000007$	3.04	293	0.0103754
	LP-SM-G3	8	10.4	$0.709475 \pm 0.000006$	2.71	603	0.0044942
jinggu	LP-SM-G1	-	14.4	$0.708648 \pm 0.000007$	1.15	186	0.0061828
	LP-SM-G2	6.9	14.4	$0.708081 \pm 0.000006$	3.47	3573	0.0009712
	LP-SM-G3	20.3	15.1	$0.708712 \pm 0.000008$	3.49	679	0.0051399
	LP-SM-G6	10.2	13.5	$0.708792 \pm 0.000010$	12.4	308	0.0402597
Mengyejing	G1	-	12.2	$0.709717 \pm 0.000007$	15.5	29.4	0.5272109
	G2	-	15.5	$0.710058 \pm 0.000006$	0.258	152	0.0016974
	G3	-	8.8	$0.710019 \pm 0.000006$	4.73	227	0.020837
	G4	4.1	8	$0.709881 \pm 0.000007$	22.5	100	0.225
	G5	10.3	9.1	$0.709937 \pm 0.000005$	37.1	163	0.2276074
	G6	-	13.9	$0.710071 \pm 0.000005$	11.6	55.4	0.2093863
Baozang	JBZ-F1	6.6	15	$0.709268 \pm 0.000006$	0.458	144	0.0031806
	JBZ-F2	6.8	14.8	$0.709225 \pm 0.000006$	0.314	154	0.002039
	JBZ-F3	7.7	15	$0.709548 \pm 0.000005$	0.363	161	0.0022547
	JBZ-F4	7.4	14.8	$0.708794 \pm 0.000005$	0.525	178	0.0029494
	JBZ-F5	-	14.3	$0.709074 \pm 0.000005$	1.25	528	0.0023674
	JBZ-G02	15.1	15.2	$0.709148 \pm 0.000009$	3.19	263	0.0121293
	JBZ-G03	13.6	14.9	$0.70855 \pm 0.000011$	0.813	222	0.0036622
	JBZ-G04	16.8	14.9	$0.708755 \pm 0.000010$	3.47	232	0.0149569
	JBZ-G05	9.1	14.9	$0.708152 \pm 0.000017$	0.962	236	0.0040763
	JBZ-G06	10.3	15.1	$0.708513 \pm 0.000020$	2	236	0.0084746
	JBZ-G07	10.2	14.9	$0.708114 \pm 0.000010$	0.154	319	0.0004828
	JBZ-G08	10.5	14.9	$0.708918 \pm 0.000011$	9.53	135	0.0705926
	JBZ-G09	16.1	15	$0.708322 \pm 0.000013$	1.05	262	0.0040076
JBZ-G10	14	14.7	$0.708242 \pm 0.000009$	0.159	195	0.0008154	
JBZ-G11	13.4	14.5	$0.708625 \pm 0.000011$	1.85	166	0.0111446	
JBZ-G12	9.7	14.6	$0.70833 \pm 0.000010$	0.078	234	0.0003333	
JBZ-G13	9	14.7	$0.708538 \pm 0.000016$	1.05	218	0.0048165	

Table 2. Cont.

Location	Sample ID	$\delta^{18}\text{O}\%$	$\delta^{34}\text{S}_{\text{V-CDT}}$	$^{87}\text{Sr}/^{86}\text{Sr}$	Rb (ppm)	Sr (ppm)	Rb/Sr
	JBZ-G14	13.3	14.2	$0.709253 \pm 0.000016$	8.93	279	0.0320072
	JBZ-G15	7.1	14.6	$0.708693 \pm 0.000018$	1.71	202	0.0084653
	JBZ-G16		14.3	$0.708672 \pm 0.000013$			#DIV/0!
	JBZ-G17	15.7	14.8	$0.708643 \pm 0.000026$	26.9	168	0.160119
	JBZ-G18	8.9	13.9	$0.708713 \pm 0.000013$	3.94	246	0.0160163
	JBZ-G19	14.8	14.6	$0.7086 \pm 0.000011$	0.517	312	0.0016571
	JBZ-G20	17.3	14.7	$0.708807 \pm 0.000017$	0.506	321	0.0015763
	JBZ-G21	10	14.4	$0.708439 \pm 0.000010$	0.757	451	0.0016785
	JBZ-G22	10	13.6	$0.708346 \pm 0.000011$	0.198	476	0.000416
	JBZ-G23	13	14.5	$0.708584 \pm 0.000009$	0.321	514	0.0006245
	JBZ-G24	8.4	14.6	$0.708523 \pm 0.000012$	10	485	0.0206186
	JBZ-G25	15.7	14.1	$0.708897 \pm 0.000013$	0.262	551	0.0004755
	JBZ-G26	9.1	14.6	$0.709085 \pm 0.000013$	1.63	248	0.0065726
	JBZ-G27	11.3	14.7	$0.709174 \pm 0.000014$	10	284	0.0352113
	JBZ-G28	9.4	14.3	$0.709184 \pm 0.000010$	3.61	302	0.0119536
	JBZ-G29	12.7	13.4	$0.709128 \pm 0.000006$	1.89	366	0.0051639
	JBZ-G30	18.4	14.3	$0.709053 \pm 0.000005$	12.2	403	0.030273
	JBZ-G31	23.7	14.2	$0.708704 \pm 0.000006$	1.21	445	0.0027191
	JBZ-G32	10	14.2	$0.709038 \pm 0.000006$	2.25	277	0.0081227
	JBZ-G33	11	14.1	$0.708781 \pm 0.000005$	1.47	491	0.0029939

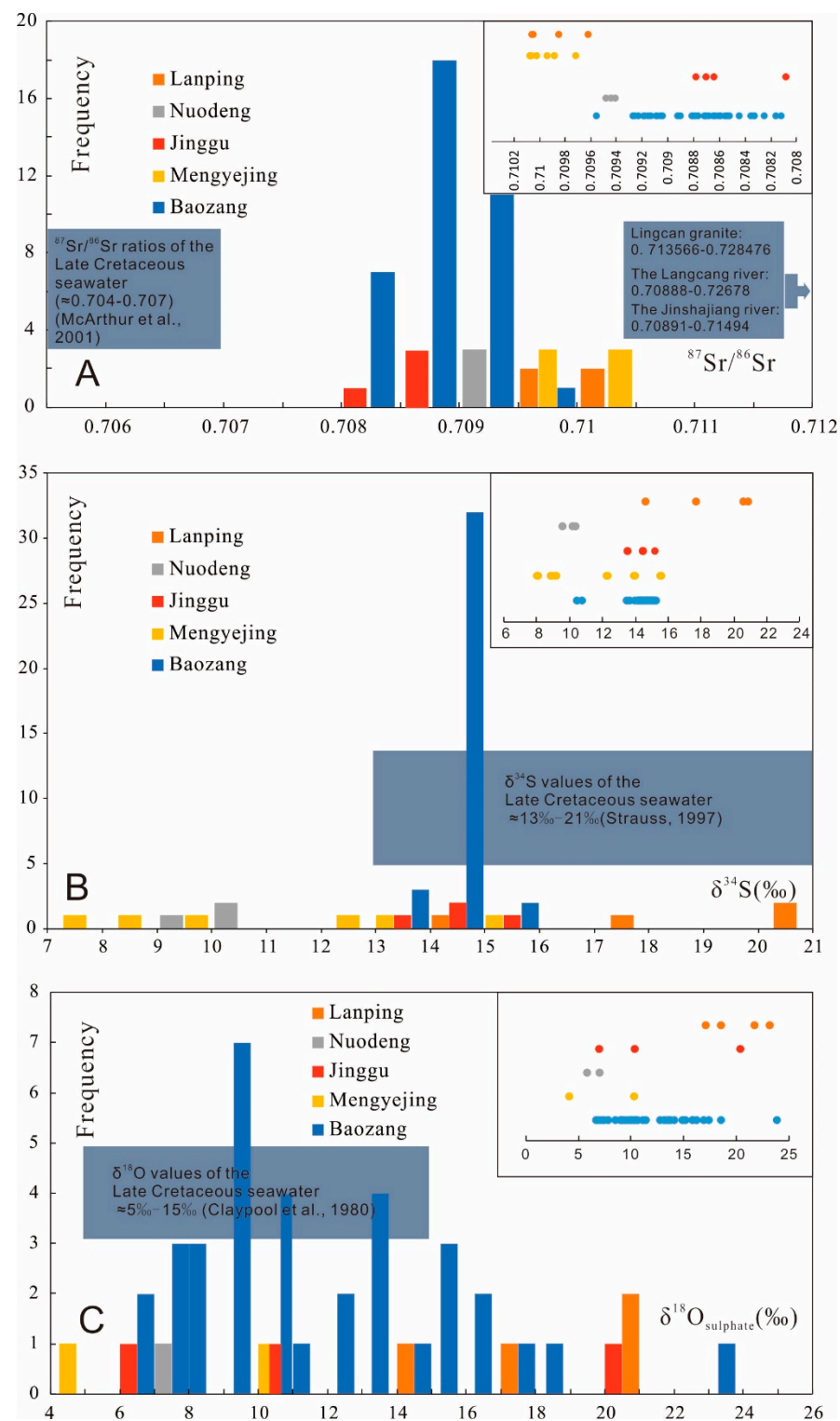


**Figure 6.** Histograms showing distribution of (A)  $^{87}\text{Sr}/^{86}\text{Sr}$  ratios, (B)  $\delta^{34}\text{S}$  values, and (C)  $\delta^{18}\text{O}$  values in evaporitic minerals from the Lanping–Simao Basin.

The sulfate samples from Baozang and Jinggu in the Simao Basin have less variable  $\delta^{34}\text{S}$  values (mean 14.6‰, S.D. = 0.4,  $n = 37$ ) than those from Lanping (mean 18.3‰, S.D. = 2.9,  $n = 4$ ), Nuodeng (mean 10.0‰, S.D. = 0.5,  $n = 3$ ), and Mengyejing (mean 11.25‰, S.D. = 3.07,  $n = 6$ ) (Table 2, Figure 6B).

The  $\delta^{18}\text{O}$  values of all samples show scattered pattern: Baozang (mean 11.89‰, S.D. = 3.85,  $n = 35$ ), Lanping (mean 20.0‰, S.D. = 2.81,  $n = 4$ ), Nuodeng (mean 7.4‰,

S.D. = 0.85, n = 2), Jinggu (mean 12.47‰, S.D. = 6.98, n = 3), Mengyejing (mean 7.2‰, S.D. = 4.38, n = 2) (Table 2, Figure 6C).

## 5. Discussion

The ages of the samples are constrained to be the Middle to Late Cretaceous (ca. 110 to 65 Ma). Albeit the uncertainty of the sedimentary ages, comparison between the S, O, and Sr isotope compositions of these samples with values of seawater [19,21,22] reveals the origin of those parent brines in which evaporite minerals were precipitated.

### 5.1. Sr Isotopes

The Sr isotope compositions of the evaporite minerals reflect the sources of Sr to the basin, together with possible interactions between the brines and rocks within the drainage basin [18]. The elevated  $^{87}\text{Sr}/^{86}\text{Sr}$  ratios of rock salts in Mengyejing (Table 2) was very likely caused by the accumulation of radiogenic  $^{87}\text{Sr}$  due to high Rb/Sr ratios (Table 2) and/or continental waters with high  $^{87}\text{Sr}/^{86}\text{Sr}$  ratios. The  $^{87}\text{Sr}/^{86}\text{Sr}$  ratios of gypsums in halite crystal fall within those of chloride salts (halite, sylvite, and carnallite, 0.708697–0.710956, except two anomalous low values [1]) in the Mengyejing potash deposit. The Rb/Sr ratios of those chloride salts are much higher than those of gypsums [1], indicating that the salt minerals in the Mengyejing potash deposit were formed by recent recrystallization process, and high Rb contents of chloride salts have not accumulated sufficient radiogenic  $^{87}\text{Sr}$  to generate higher  $^{87}\text{Sr}/^{86}\text{Sr}$  ratios compared with gypsums.

The influence of radiogenic  $^{87}\text{Sr}$  on gypsum samples was negligible because of the extremely low Rb/Sr ratios (Table 2). Thus, the Sr isotope composition of gypsum could represent the Sr isotopic signature of parent brine in which gypsum precipitated. The  $^{87}\text{Sr}/^{86}\text{Sr}$  ratios of all gypsum samples shown in Table 2 and Figure 7 are higher than the range of coeval seawaters [22]. This is consistent with the conclusion that the  $^{87}\text{Sr}/^{86}\text{Sr}$  ratios of evaporites in continental setting are generally higher than those of seawater [32]. Apparently, the parent brines were derived, at least partly, from continental water. The weathering of the Lincang granite (Figure 1) could have supplied dissolved components with high  $^{87}\text{Sr}/^{86}\text{Sr}$  ratios. The  $^{87}\text{Sr}/^{86}\text{Sr}$  ratios of biotite granite in Lincang range from 0.730006 to 0.743494, corresponding to an initial  $^{87}\text{Sr}/^{86}\text{Sr}$  ratio range of 0.713566 to 0.728476 when granite formed during Triassic based on Rb/Sr ratios [33]. In addition to the Lincang granite, other regions may have provided weathering products with varying Sr isotope compositions. The Sr isotope compositions and Sr concentrations of those continental waters were unknown. We postulate that the continental freshwater had similar Sr concentration and Sr isotopic ratios to those of present river water. Noh et al. (2009) [34] presented Sr concentrations and isotope compositions of two major rivers enclosing the Lanping–Simao Basin: The Jinshajiang River, 0.33–11.46  $\mu\text{M}$ ,  $^{87}\text{Sr}/^{86}\text{Sr} = 0.70891\text{--}0.71494$ , and the Lancang River, 0.28–6.73  $\mu\text{M}$ ,  $^{87}\text{Sr}/^{86}\text{Sr} = 0.70888\text{--}0.72678$ . The low Sr concentrations of river waters necessitate a large amount of continental fluvial input to produce the elevated  $^{87}\text{Sr}/^{86}\text{Sr}$  ratios of gypsums in the Lanping–Simao Basin.

The  $^{87}\text{Sr}/^{86}\text{Sr}$  ratios of ankerites within the Mesozoic strata in the Lanping–Simao Basin range from 0.70874 to 0.71332 [35]. The brines in which those ankerites precipitated were thought to have been formed by circulation of basinal fresh waters. Sr was leached out from Mesozoic strata [35], thus the  $^{87}\text{Sr}/^{86}\text{Sr}$  ratios of ankerites could represent those of the Mesozoic sedimentary rocks. Consequently, it is likely that the parent brine for forming evaporites could also have derived from adjacent clastic rocks to some extent.

As a whole, the Sr isotope compositions of gypsums in the Lanping Basin are higher than those of gypsums in the Simao Basin. Recent provenance studies show that the Late Cretaceous sediments from these basins have an overall S-directed paleocurrent that flowed from the Lanping Basin to the Simao Basin [36]. The Lanping Basin could have trapped more continental waters compared with the Simao Basin.

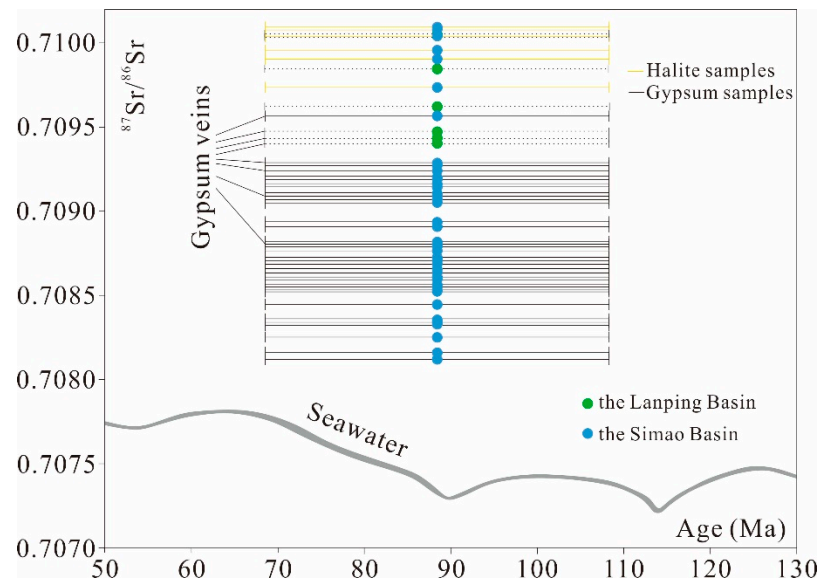


**Figure 7.** Comparison between  $^{87}\text{Sr}/^{86}\text{Sr}$  ratios of evaporite minerals in Lanping–Simao Basin and contemporaneous seawater (data from [22]).

5.2. S Isotopes

The  $\delta^{34}\text{S}$  values of gypsum laminae samples in Baozang show a narrow range, from 13.4‰ to 15.2‰ (Table 2, Figure 8) which is consistent with those of Cretaceous seawater [19,21]. Wang et al. (2014a) [12] implied that there was a marine transgression during the Late Cretaceous based on geochemical, palaeogeographical, and paleomagnetic studies ([12] and references therein). The crystal of vein-shaped gypsum was corroded and dissolved by external fluids or internal waters from dehydration of gypsum (Figure 5I), indicating that vein-shaped gypsums had undergone dissolution and recrystallization process. The secondary veined gypsum samples in Baozang have similar S isotope compositions to those of bedded gypsum samples (Table 2), denoting that the sulfate-bearing fluids for forming the secondary veined gypsums mainly stemmed from the dissolution of bedded gypsums.

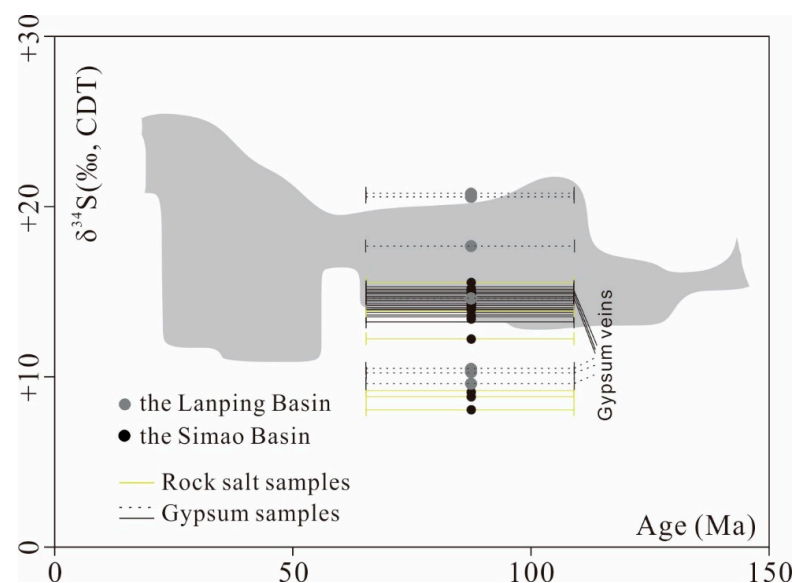


**Figure 8.** Comparison between  $\delta^{34}\text{S}$  values of sulfates in the Lanping–Simao Basin and contemporaneous seawater (data from [21]).

The  $\delta^{34}\text{S}$  values of rock salt samples in Mengyejing range from 8.0‰ to 15.5‰, which are slightly lower than those of gypsum samples near Mengyejing (Baozang). During evaporation,  $^{34}\text{S}$  and  $^{18}\text{O}$  are enriched in precipitated gypsum and relatively depleted in brines. Therefore, when a restricted basin is not supplied by open water, the progressive evaporation process would have resulted in reduced  $\delta^{34}\text{S}$  and  $\delta^{18}\text{O}$  values of residual brine and subsequent precipitated gypsum, namely, reservoir effect [37]. Thus, the reduced  $\delta^{34}\text{S}$  values of sulfates in rock salt samples in Mengyejing was likely caused by reservoir effect. Besides, dissolved sulfates in continental waters with lower  $\delta^{34}\text{S}$  values could have contributed to the brine in the final stage of evaporation. The assemblage of predominant halite crystals with a trace amount of euhedral gypsum and sylvite crystal (Figure 5K,L) indicates a very saline stage during which both reservoir effect and continental input could result in the lowering of  $\delta^{34}\text{S}$  values. This process may have changed the  $\delta^{34}\text{S}$  values more efficiently because of the low sulfate concentration of brine in the final stage of evaporation.

The  $\delta^{34}\text{S}$  values of gypsum samples in Jinggu are consistent with those of gypsum samples in Baozang, indicating a similar marine origin due to the Cretaceous marine transgression. Gypsum laminae (Figure 4F) and amenoid microcrystalline gypsums (Figure 5E) suggest a likely primary origin. However, the anhydrite relics with surrounding gypsum crystals (Figure 5F) indicate that dehydration of gypsum and hydration of anhydrite cycle have occurred. The S isotopes of sulfates suggests that the dehydration–hydration process did not affect the isotopic signatures significantly.

In Lanping,  $\delta^{34}\text{S}$  values of two gypsum samples are 14.5‰ and 17.6‰, respectively; slightly higher than those of Cretaceous seawater and gypsum samples in the Simao Basin. Two celestite samples have  $\delta^{34}\text{S}$  values ranging from 20.5‰ to 20.7‰, which are much higher than those of gypsum samples. Reservoir effect and continental contribution could lower the  $\delta^{34}\text{S}$  values, which is not the case here. Therefore, the elevated  $\delta^{34}\text{S}$  values of gypsum and celestite samples in Lanping could have contributed to other factor(s), such as bacterial sulfate reduction (BSR). During BSR, the lighter isotopes  $^{32}\text{S}$  and  $^{16}\text{O}$  are preferentially metabolized by microorganisms, causing an enrichment of heavy isotopes  $^{34}\text{S}$  and  $^{18}\text{O}$  in the remaining sulfate [38]. Organic matters are widely distributed in the Jinding Pb-Zn deposit in Lanping area. In reducing environment, sulfates were reduced to sulfides. Pyrite is commonly developed in gypsums (Figure 5B). It was suggested that  $\text{S}^{2-}$  in sulfides (mainly consist of sphalerite and galena) were generated by sulfate reduction [3] and resulted in  $^{34}\text{S}$ -enriched fluids. The euhedral celestite crystal (Figure 5C) could have been formed by  $^{34}\text{S}$ -enriched fluids in combination with Sr-bearing metal fluids. Gypsums and celestites are distributed within the Triassic marine sequence in Lanping area with  $\delta^{34}\text{S}$  values ranging from 15.3‰ to 17.5‰ [39]. It was possible that the recycling of Triassic evaporites could have contributed and affected the composition of S isotopes of evaporites formed in the non-marine setting during Cretaceous.

The reduced  $\delta^{34}\text{S}$  values of gypsum samples in Nuodeng were not controlled by BSR. It was not likely caused by reservoir effect either because it engenders negligible depletion of  $^{34}\text{S}$  in sulfates during gypsum precipitation stage [37]. Therefore, only continental input with isotopically light  $^{32}\text{S}$  could account for this result. The Jinding Pb-Zn deposit comprises a great amount of sulfide minerals, including sphalerite and galena. Approximately 600 million tons of Pb + Zn were eroded [39]. The sulfide minerals show a wide range of  $\delta^{34}\text{S}$  values, from  $-54.9\text{‰}$  to  $+3.5\text{‰}$  [39]. The  $\delta^{34}\text{S}$  values of sulfates formed via sulfide oxidation are generally equivalent to those of the parent sulfide minerals [40]. There is no or insignificant fractionation during the oxidation process of sulfide. Nuodeng is only 60 km to the south of Lanping. Weathering products of the Jinding Pb-Zn deposit could be easily transported from Lanping to Nuodeng. The re-oxidation of reduced sulfides with low  $\delta^{34}\text{S}$  values resulted in relatively low sulfate  $\delta^{34}\text{S}$  values in Nuodeng.

A giant marine evaporite deposit occurred within the Maha Sarakham Formation, the Khorat Basin, Thailand. Qu (1998) [10] suggested that the evaporites within the Lanping–Simao Basin have a close relationship with evaporites within the Khorat Basin based on sedimentary sequences comparison and salt mineral assemblages. The  $\delta^{34}\text{S}$  values of

anhydrites intercalated with rock salt layers within the Maha Sarakham evaporite deposit range from 14.8‰ to 17.7‰ [41]. The  $\delta^{34}\text{S}$  values of layered anhydrite in Baozang are consistent with those of anhydrites in the Khorat Basin. Qin et al. (2020) [42] proposed a Cretaceous seawater recharge model that the paleoseawater flowed from Bangong–Nujiang Ocean (West Meso-Tethys Ocean) through the Qiangtang and Lhasa blocks to the Lanping–Simao Basin and the Khorat Basin. Alternatively, the paleoseawater could have derived from East Meso-Tethys Ocean and recharged the Lanping–Simao and Khorat Basins through Tengchong–Baoshan Blocks [42].

### 5.3. O Isotopes

The history of seawater  $\delta^{18}\text{O}_{\text{sulfate}}$  is less well-defined compared with S and Sr isotope compositions [18]. Thus, the  $\delta^{34}\text{S}$ – $\delta^{18}\text{O}$  relationships are presented for the comparison with S and O isotope values of Cretaceous seawater [19]. The global isotopic evolution through time of marine sulfates has been well documented worldwide. The oxygen isotopic compositions of sulfates from Mesozoic to present-day are within a range of approximately +10‰ to +15‰ [19]. The S vs. O isotope compositions of sulfates in the Lanping–Simao Basin are widely scattered, only a small part of samples has S vs. O isotope compositions overlapping those of seawater (Figure 9). The  $\delta^{18}\text{O}$  values of all samples show a more scattered and variable pattern compared with  $\delta^{34}\text{S}$  values (Figure 9). And the  $\delta^{34}\text{S}$  values do not co-vary with the  $\delta^{18}\text{O}$  values, indicating that different processes control the S and O isotopes of sulfate.

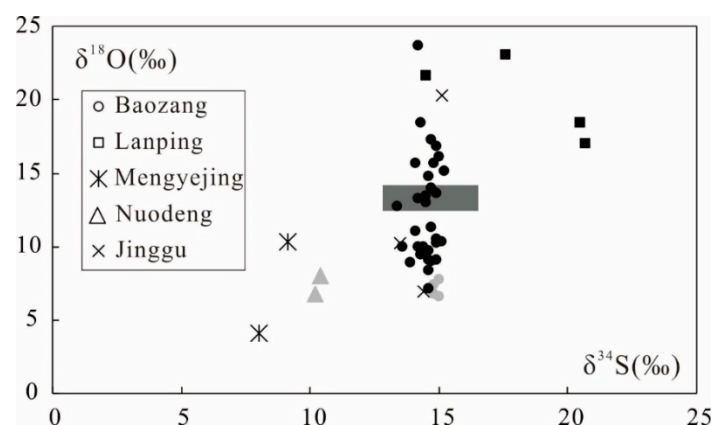


**Figure 9.** S–O isotopic compositions of evaporites in the Lanping–Simao Basin. The shaded box represents S–O isotopic compositions of marine gypsums of the Late Cretaceous period [19]. The dark black symbols indicate layered gypsum samples, whereas grey symbols indicate veined gypsum samples.

In Baozang, the narrow range of  $\delta^{34}\text{S}$  values suggests that the inflow of dissolved sulfates in the continental waters was insignificant. Because in general cases, sulfates from continental waters will add light sulfur and  $\delta^{34}\text{S}$  values decreases accordingly [37]. As discussed above, S isotope compositions of gypsum samples in Baozang denote a marine origin. S and O isotope compositions of marine sulfates are insensitive to minor non-marine contributions because seawater hosts much higher  $\text{SO}_4$  concentration than most freshwaters [43], and dissolution of sulfates results in little or negligible isotopic fractionation of S and O [19,44]. Thus, the variation of O isotope compositions of those gypsum samples was not controlled by inflow of continental dissolved sulfates and dissolution process. The scattered O isotope compositions could not either be accounted for by reservoir effect which fails to induce such a wide variation.

The changes in oxygen isotopic composition of sulfate are related to more complex processes than those affecting sulfur isotopes [45]. In a restricted basin, BSR process produced sulfides with relatively negative  $\delta^{34}\text{S}$  values and residual dissolved sulfates with positive  $\delta^{34}\text{S}$  values. The resulted sulfides from BSR diffused into shallow water and reoxidized to sulfates with the incorporation of O from water and/or molecular oxygen [45].



Sulfates formed by re-oxidation of sulfide would cause no fractionation on S but varied fractionation on  $^{18}\text{O}$  through the incorporation of dissolved oxygen and/or oxygen of hypersaline water [46]. In the presence of molecular oxygen, the  $\delta^{18}\text{O}$  value of the resulting sulfate oxidized by sulfide is considered to shift towards heavy values. Whereas, under anaerobic conditions, the oxidation of sulfide yields a sulfate with isotopically light  $\delta^{18}\text{O}$  values equal or very close to that of environmental water [45]. Moreover, the exchange of oxygen atoms of intermediate anions like  $\text{SO}_3^{2-}$  and/or  $\text{HSO}_3^-$  complicates the oxidation processes that may affect the final O isotope composition of sulfate. The proportions of water-derived oxygen and molecular oxygen incorporated into sulfates during the re-oxidation process of sulfide were subject to environments ([47] and references therein). Mangalo et al. (2007) [48] performed an experiment which proved that the  $\delta^{18}\text{O}$  value of sulfate during BSR could be affected by isotope exchange with water. They supported a fractionation mechanism of re-oxidation of sulfite to sulfate rather than that of reaction from sulfate-enzyme complex back to sulfate ([48] and references therein).

At the water-sediment interface, the constant cycling between sulfate reduction and sulfide reoxidation has no net effect on the burial of reduced sulfur, but greatly affects the oxygen isotope composition of marine sulfate ( $\delta^{18}\text{O}_{\text{SO}_4}$ ; [49] and references therein). Therefore, this redox cycle of sulfur only affects the sulfate O-isotope ratio significantly, but not the sulfate S-isotope ratio [50,51]. The S vs. O pattern of sulfates in Baozang is consistent with that produced by sulfate reduction and sulfide re-oxidation process.

Organic matters were widely distributed in the Lanping–Simao Basin, usually presented as debris (Lanping, Nuodeng, Baozang, and Mengyejing, Figure 4L) and/or banded layer (Lanping and Jinggu) [52]. It was very likely that BSR occurred under anoxic conditions and sulfates were reduced to sulfides. The sulfides were then re-oxidized in the “red bed” environment. This process causes little variation on S isotope compositions if there was no extraneous S. Whereas, reduction-re-oxidation process changes the O isotope compositions of sulfates drastically under different environments.

The S-O isotope compositions of sulfates in rock salt samples from Mengyejing are located to the lower left of marine isotope compositions (Figure 9). This pattern could have been the result of reservoir effect and/or reduction-re-oxidation process. It is practically impossible to determine what process(es) was predominant.

The S-O isotope compositions of sulfates from Lanping are located to the upper right of marine isotope compositions (Figure 9), which are similar to those of Messinian gypsums in the Nijr Basin [53]. The elevated  $\delta^{34}\text{S}$  and  $\delta^{18}\text{O}$  values resulted by redox cycling involving BSR and re-oxidation in stratified brines [53]. BSR produced a great amount of  $\text{S}^{2-}$  which incorporated into metal cations and formed metal sulfides in Lanping. The residual sulfates would be enriched in  $^{34}\text{S}$  and  $^{18}\text{O}$ .

#### 5.4. The Origin of Evaporites and Paleoenvironmental Significance

Although Sr isotope compositions of all samples and S isotope compositions of samples from Nuodeng corroborate a major continental contribution to the formation of the evaporites, S isotope compositions of sulfates from Lanping, Jinggu, and Baozang indicate a marine origin. Trace elements of chloride salts in the Mengyejing potash deposit also suggested a marine contribution [15]. In conclusion, the parent brine in which evaporite minerals precipitated were derived from a mixture of seawater and continental waters.

In Baocang, the narrow range of  $\delta^{34}\text{S}$  values vs. wide range of  $^{87}\text{Sr}/^{86}\text{Sr}$  (Figure 10) indicate that continental input imposes a greater effect on Sr than on S. The seawater dominated in terms of S isotopes, whereas continental input controlled the Sr isotopes. In Jinggu, the  $^{87}\text{Sr}/^{86}\text{Sr}$  ratios vs.  $\delta^{34}\text{S}$  values show a similar pattern to that of evaporites in Baozang, which suggest a similar origin and formation process. In Mengyejing, the  $^{87}\text{Sr}/^{86}\text{Sr}$  ratios are relatively steady but  $\delta^{34}\text{S}$  values show a large variation. This pattern indicates that reservoir effect controlled the S isotopes which is consistent with preceding discussion. In Nuodeng, the low  $\delta^{34}\text{S}$  values, high  $^{87}\text{Sr}/^{86}\text{Sr}$  ratios, and limited distribution of S vs. Sr suggest that the parent brines were only controlled by continental waters derived

from weathering. In Lanping, the positive relationship between the  $^{87}\text{Sr}/^{86}\text{Sr}$  ratios and the  $\delta^{34}\text{S}$  values indicates that the formation of evaporites could have been controlled by continental influx, recycle of older evaporites, and BSR synergistically.

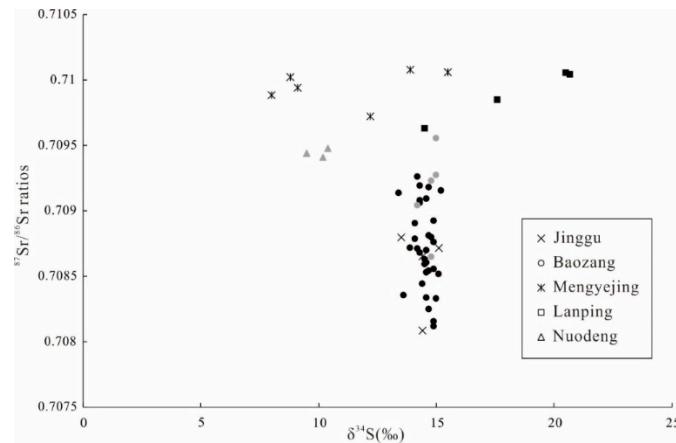


**Figure 10.** Sr-S isotopic compositions of evaporites in the Lanping–Simao Basin. The dark black symbols indicate layered gypsum samples, whereas grey symbols indicate veined gypsum samples.

The  $\delta^{18}\text{O}$  values,  $\delta^{34}\text{S}$  values, and  $^{87}\text{Sr}/^{86}\text{Sr}$  ratios of gypsum laminae samples from a single section in Baozang (Figure 11) show that: (1) the  $^{87}\text{Sr}/^{86}\text{Sr}$  ratios fluctuate more drastically than  $\delta^{34}\text{S}$  values; (2) although the  $^{87}\text{Sr}/^{86}\text{Sr}$  ratios are fluctuant, a roughly increasing trend is identifiable from base to top; (3) the  $\delta^{34}\text{S}$  values yields a mirror image pattern of  $^{87}\text{Sr}/^{86}\text{Sr}$  ratios, i.e., a decreasing trend in  $\delta^{34}\text{S}$  values from base to top; (4)  $\delta^{18}\text{O}$  values pattern is scattered and not related to Sr and S isotopes.

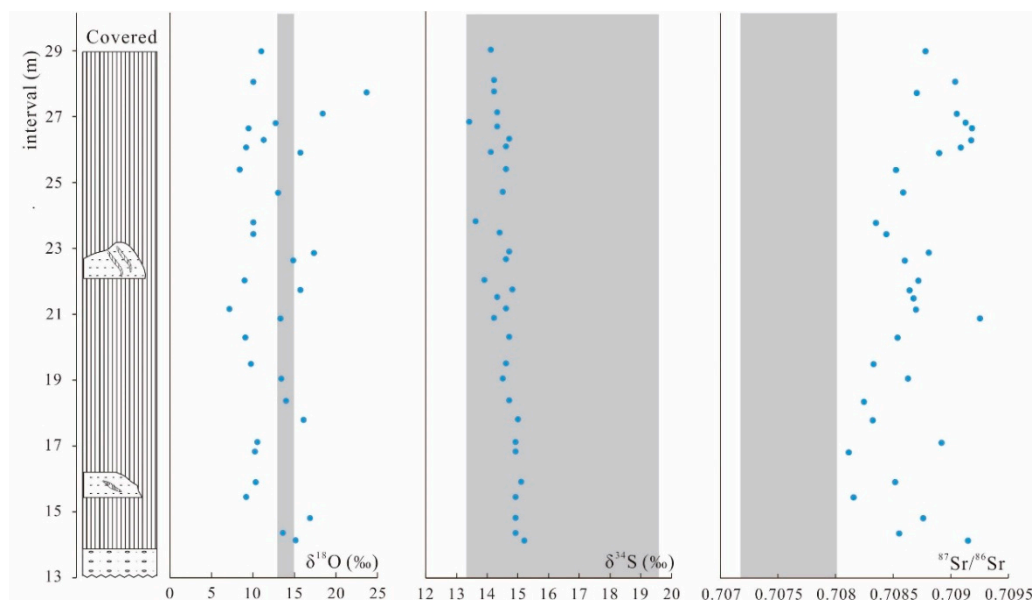


**Figure 11.** Variations of  $\delta^{18}\text{O}$  values,  $\delta^{34}\text{S}$  values, and  $^{87}\text{Sr}/^{86}\text{Sr}$  ratios of gypsum samples from the section in Baozang. Shaded area:  $\delta^{18}\text{O}$  values [19],  $\delta^{34}\text{S}$  values [21], and  $^{87}\text{Sr}/^{86}\text{Sr}$  ratios [22] of contemporaneous marine sulfates.

Kristall et al. (2018) [54] suggested that continental input dominates Sr and S isotopic signature when  $^{87}\text{Sr}/^{86}\text{Sr}$  ratios and  $\delta^{34}\text{S}$  values shift in opposition. In this section, the decreasing trend of  $\delta^{34}\text{S}$  values in combination with the increasing trend of  $^{87}\text{Sr}/^{86}\text{Sr}$  ratios suggest that continental input played an increasingly significant role with the progressive evaporation of brines. We suggest that the major waterbody for forming the evaporites were

remnant seawater due to marine transgression. In the late stage of evaporation, continental waters played a more important role and predominated with respect to isotope signatures.

As discussed above, redox conditions, O isotope compositions of parent brine, and molecular O could determine the final O isotope compositions of dissolved sulfate, thus complicating the O isotope compositions of precipitated sulfates. The greatly varied S and O isotope compositions of gypsums in Messinian evaporites [55] may result from repeated processes of evaporite dissolution and re-precipitation as well as from bacterial activities during redox variations [45,56]. The wide variation of O isotopes compositions of gypsums in such a short section (15 m) in Baozang also suggests a drastic sedimentary environmental change during evaporite deposition. S and O isotope compositions of gypsums in Jinggu have a similar pattern to that of in Baozang, denoting a similar process.

## 6. Conclusions

- (1) The  $^{87}\text{Sr}/^{86}\text{Sr}$  ratios of sulfate samples (including gypsum and celestite) in the Lanping–Simao basin are higher than those of contemporaneous seawater, indicating continental contribution; elevated  $^{87}\text{Sr}/^{86}\text{Sr}$  ratios of rock salt samples were caused by continental contribution and radiogenic  $^{87}\text{Sr}$  accumulation.
- (2) The  $\delta^{34}\text{S}$  values of gypsum samples in the Simao basin are consistent with those of Cretaceous seawater, suggesting a marine origin; the reduced  $\delta^{34}\text{S}$  values of rock salt samples might be due to reservoir effect and continental contribution; the relatively higher  $\delta^{34}\text{S}$  values of sulfates in Lanping were likely caused by BSR or/and recycling of Triassic sulfates; the low  $\delta^{34}\text{S}$  values of gypsums in Nuodeng was caused by re-oxidation of weathering sulfides with negative S isotope compositions.
- (3) Sr and S isotope compositions of gypsum samples in a single section in Baozang suggest that continental water played an increasingly significant role with the evaporation of brines.
- (4) The O isotope compositions of evaporite salts showing more complex pattern compared with Sr and S, indicating that sulfate reduction or/and re-oxidation processes prevailed during deposition.

In summary, the parent brines in which evaporites precipitated within the Mesozoic “red bed” of the Lanping–Simao Basin mainly stemmed from remnant seawater due to marine transgression and continental water. During the evaporation, the paleoenvironment changed dramatically based on O isotopic compositions of sulfates, and continental water played an increasingly important role compared with remnant seawater.

**Author Contributions:** L.S. and L.W. wrote the paper. L.W., C.L., and Y.Z. investigated and collected the samples. L.W. and L.S. obtained and processed the chemical, isotopic, XRD, SEM data. All authors have read and agreed to the published version of the manuscript.

**Funding:** This work is supported by the National Key Project for Basin Research of China (2011CB403007), the National Natural Science Foundation of China (41572067, 91855104, 41802111).

**Institutional Review Board Statement:** Not applicable.

**Informed Consent Statement:** Not applicable.

**Data Availability Statement:** Not applicable.

**Acknowledgments:** We are grateful to Jianfu Fan for his assistance in sampling and Hongwei Li, Changfu Fan, and Bin Hu for his data processing.

**Conflicts of Interest:** The authors declare no conflict of interest.

## References

1. Shen, L.; Liu, C.; Zhao, J.; Feng, Y.; Wang, L.; Zhou, J. The remaking of the Mengyejing potash deposit in Yunnan, China: Evidence from Rb–Sr isotopic systematics. *Ore Geol. Rev.* **2017**, *89*, 876–886. [[CrossRef](#)]
2. Xue, C.; Zeng, R.; Liu, S.; Chi, G.; Qing, H.; Chen, Y.; Yang, J.; Wang, D. Geologic, fluid inclusion and isotopic characteristics of the Jinding Zn–Pb deposit, western Yunnan, South China: A review. *Ore Geol. Rev.* **2007**, *31*, 337–359. [[CrossRef](#)]

3. Hu, G.Y.; Li, Y.H.; Zeng, P.S. The role of halosalt in mineralization of the Jinding Pb-Zn deposit: Evidence from sulphur and strontium isotopic compositions. *Acta Geol. Sin.* **2013**, *87*, 1694–1702. (In Chinese)
4. Deng, J.; Wang, Q.; Li, G.; Santosh, M. Cenozoic tectono-magmatic and metallogenic processes in the Sanjiang region, southwestern China. *Earth Sci. Rev.* **2014**, *138*, 268–299. [[CrossRef](#)]
5. Leach, D.L.; Song, Y.C.; Hou, Z.Q. The world-class Jinding Zn–Pb deposit: Ore formation in an evaporite dome, Lanping Basin, Yunnan, China. *Miner. Deposita.* **2017**, *52*, 281–296. [[CrossRef](#)]
6. Xia, W.; Li, X. about the theoretic original study of evaporites-from the potash-halite deposit in Mengyejing Yunnan. *J. Miner. Pet.* **1983**, *3*, 1–11. (In Chinese)
7. Shuai, K. Geologic-Tectonic evolution and evaporite formation of Mesozoic-Cenozoic era in Yunnan. *Geoscience* **1987**, *1*, 207–227. (In Chinese)
8. Gao, G. Review of geological origin about Jinding lead-zinc ore deposit. *Earth Sci. J. China Univ. Geosci.* **1989**, *14*, 467–475. (In Chinese)
9. Gao, G. Formation age and involved problems on anhydrites ore in Jinding lead-zinc ore area. *Yunnan Geol.* **1991**, *10*, 191–206. (In Chinese)
10. Qu, Y.; Yuan, P.; Shuai, K.; Zhang, Y.; Cai, K.; Jia, S.; Chen, C. *Potash-forming Rules and Prospects of Lower Tertiary in Lanping–Simao Basin, Yunnan*; Geological Publishing House: Beijing, China, 1998; pp. 1–120. (In Chinese)
11. Gao, X.; Fang, Q.; Yao, W.; Peng, Q.; Dong, J.; Qin, H.; Di, Y. Genesis of the Mengyejing potash deposit in Lanping-Simao basin, Yunnan: Implication from the components of the deposit. *Acta Geosci. Sin.* **2013**, *34*, 529–536. (In Chinese)
12. Wang, L.; Liu, C.; Fei, M.; Shen, L.; Zhang, H. Sulfur isotopic composition of sulfate and its geological significance of the Yunlong formation in the Lanping Basin, Yunnan Province. *China Min. Mag.* **2014**, *23*, 57–65. (In Chinese)
13. Shen, L.; Liu, C.; Wang, L.; Hu, Y.; Hu, M.; Feng, Y. Degree of Brine Evaporation and Origin of the Mengyejing Potash Deposit: Evidence from Fluid Inclusions in Halite. *Acta Geol. Sin.* **2017**, *91*, 175–185. (In English) [[CrossRef](#)]
14. Zhang, J.; Wen, H.; Qiu, Y.; Zhang, Y.; Li, C. Ages of sediment-hosted Himalayan Pb–Zn–Cu–Ag polymetallic deposits in the Lanping basin, China: Re–Os geochronology of molybdenite and Sm–Nd dating of calcite. *J. Asian Earth Sci.* **2013**, *73*, 284–295. [[CrossRef](#)]
15. Xu, X.; Wu, J. Potash deposits in Mengyejing, Yunnan-A study of certain characteristics, geochemistry of trace elements and genesis of the deposits. *Bull. Chin. Acad. Geol. Sci.* **1983**, *5*, 17–36. (In Chinese)
16. Li, M.; Yan, M.; Wang, Z.; Liu, X.; Fang, X.; Li, J. The origins of the Mengye potash deposit in the Lanping–Simao basin, Yunnan province, Western China. *Ore Geol. Rev.* **2015**, *69*, 174–186. [[CrossRef](#)]
17. Liu, C.; Wang, L.; Yan, M.; Zhao, Y.; Cao, Y.; Fang, X.; Shen, L.; Wu, C.; Lv, F.; Ding, T. The Mesozoic-Cenozoic tectonic settings, paleogeography and evaporitic sedimentation of Tethyan blocks within China: Implications for potash formation. *Ore Geol. Rev.* **2018**, *102*, 406–425. [[CrossRef](#)]
18. Palmer, M.R.; Helvacı, C.; Fallick, A.E. Sulphur, sulphate oxygen and strontium isotope composition of Cenozoic Turkish evaporites. *Chem. Geol.* **2004**, *209*, 341–356. [[CrossRef](#)]
19. Claypool, G.E.; Holser, W.T.; Kaplan, I.R.; Sakai, H.; Zak, I. The age curves of sulfur and oxygen isotopes in marine sulfate and their mutual interpretation. *Chem. Geol.* **1980**, *28*, 199–260. [[CrossRef](#)]
20. Veizer, J. Strontium isotopes in seawater through time. *Annu. Rev. Earth Planet. Sci. Lett.* **1989**, *17*, 141–167. [[CrossRef](#)]
21. Strauss, H. The isotopic composition of sedimentary sulfur through time. *Palaeogeogr. Palaeoclimatol. Palaeoecol.* **1997**, *132*, 97–118. [[CrossRef](#)]
22. McArthur, J.M.; Howarth, R.J.; Bailey, T.R. Strontium isotope stratigraphy: LOWESS version 3: Best fit to the marine Sr-isotope curve for 0–509 Ma and accompanying look-up table for deriving numerical age. *J. Geol.* **2001**, *109*, 155–170. [[CrossRef](#)]
23. Kampschulte, A.; Strauss, H. The sulfur isotopic evolution of Phanerozoic seawater based on the analysis of structurally substituted sulfate in carbonates. *Chem. Geol.* **2004**, *204*, 255–286. [[CrossRef](#)]
24. Alonso-Azcárate, J.; Bottrell, S.H.; Mas, J.R. Synsedimentary versus metamorphic control of S, O and Sr isotopic compositions in gypsum evaporites from the Cameros Basin, Spain. *Chem. Geol.* **2006**, *234*, 46–57. [[CrossRef](#)]
25. Metcalfe, I. Palaeozoic-Mesozoic history of SE Asia. *Geol. Soc. Lond. Spec. Publ.* **2011**, *355*, 7–35.
26. Chen, H.H.; Dobson, J.; Heller, F.; Hao, J. Paleomagnetic evidence for clockwise rotation of the Simao region since the Cretaceous: A consequence of India–Asia collision. *Earth Planet Sci. Lett.* **1995**, *134*, 203–217.
27. Wang, L.; Liu, C.; Fei, M.; Shen, L.; Zhang, H.; Zhao, Y. First SHRIMP U–Pb zircon ages of the potash-bearing Mengyejing formation, Simao Basin, southwestern Yunnan, China. *Cretac. Res.* **2015**, *52*, 238–250. [[CrossRef](#)]
28. Chen, K. Provenance Analysis of the Late Cretaceous Yunlong Formation in the Lanping Basin, Yunnan Province and Its Tectonic Implications. Master’s Dissertation, China University of Geosciences, Beijing, China, 2017. (In Chinese).
29. Wang, L.C.; Shen, L.J.; Liu, C.L.; Chen, K.; Ding, L.; Wang, C.S. The Late Cretaceous source-to-sink system at the eastern margin of the Tibetan Plateau: Insights from the provenance of the Lanping Basin. *Geosci. Front.* **2021**, *12*, 101102. [[CrossRef](#)]
30. Babechuk, M.G.; Kamber, B.S. An estimate of 1.9 Ga mantle depletion using the high-field-strength elements and Nd–Pb isotopes of ocean floor basalts, Flin Flon Belt, Canada. *Precambrian Res.* **2011**, *189*, 114–139. [[CrossRef](#)]
31. Niu, Y.; Batiza, R. Trace element evidence from seamounts for recycled oceanic crust in the Eastern Pacific mantle. *Earth Planet Sci. Lett.* **1997**, *148*, 471–483. [[CrossRef](#)]

32. Denison, R.E.; Kirkland, D.W.; Evans, R. Using strontium isotopes to determine the age and origin of gypsum and anhydrite beds. *J. Geol.* **1998**, *106*, 1–18. [[CrossRef](#)]
33. Cong, F.; Wu, F.Y.; Li, W.C.; Mou, C.L.; Huang, X.M.; Wang, B.D.; Hu, F.Y.; Peng, Z.M. Origin of the Triassic Lincang granites in the southeastern Tibetan Plateau: Crystallization from crystal mush. *Lithos* **2020**, *360–361*, 105452. [[CrossRef](#)]
34. Noh, H.; Huh, Y.; Qin, J.; Ellis, A. Chemical weathering in the Three Rivers region of Eastern Tibet. *Geochim. Cosmochim. Acta* **2009**, *73*, 1857–1877. [[CrossRef](#)]
35. Xiao, R.; Chen, H.; Shuai, K.; Yang, Z. Mineralization of Jinman copper deposit in Mesozoic sedimentary rocks in Lanping, Yunnan Province. *Geoscience* **1994**, *8*, 490–496. (In Chinese)
36. Wang, L.; Liu, C.; Gao, X.; Zhang, H. Provenance and paleogeography of the Late Cretaceous Mengyejing Formation, Simao Basin, southeastern Tibetan Plateau: Whole-rock geochemistry, U-Pb geochronology, and Hf isotopic constraints. *Sediment. Geol.* **2014**, *304*, 44–58. [[CrossRef](#)]
37. Holser, W.T.; Kaplan, I.R. Isotope geochemistry of sedimentary sulfates. *Chem. Geol.* **1966**, *1*, 93–135. [[CrossRef](#)]
38. Kaplan, I.R.; Rittenberg, S.C. Microbiological fractionation of sulphur isotopes. *Microbiology* **1964**, *34*, 195–212. [[CrossRef](#)]
39. Zeng, P.; Li, H.; Li, Y.; Wang, Z.; Wen, L.; Liu, S. Asian largest lead-zinc ore deposit: The Jinding giant Pb-Zn deposit by three stages superimposed mineralization. *Acta Geol. Sin.* **2016**, *90*, 2384–2397. (In Chinese)
40. Taylor, B.E.; Wheeler, M.C.; Nordstrom, D.K. Stable isotope geochemistry of acid mine drainage: Experimental oxidation of pyrite. *Geochim. Cosmochim. Acta* **1984**, *48*, 2669–2678. [[CrossRef](#)]
41. El Tabakh, M.; Utha-Aroon, C.; Schreiber, B.C. Sedimentology of the Cretaceous Maha Sarakham evaporites in the Khorat Plateau of northeastern Thailand. *Sediment. Geol.* **1999**, *123*, 31–62. [[CrossRef](#)]
42. Qin, Z.; Li, Q.; Zhang, X.; Fan, Q.; Wang, J.; Du, Y.; Ma, Y.; Wei, H.; Yuan, Q.; Shan, F. Origin and recharge model of the Late Cretaceous evaporites in the Khorat Plateau. *Ore Geol. Rev.* **2020**, *116*, 103226. [[CrossRef](#)]
43. Lu, F.H.; Meyers, W.J. Sr, S, and O<sub>SO4</sub> isotopes and the depositional environments of the upper Miocene evaporites, Spain. *J. Sediment. Res.* **2003**, *73*, 444–450. [[CrossRef](#)]
44. Rick, B. Sulphur and oxygen isotopic composition of Swiss Gipskeuper (Upper Triassic). *Chem. Geol. Isot. Geosci.* **1990**, *80*, 243–250. [[CrossRef](#)]
45. Longinelli, A.; Flora, O. Isotopic composition of gypsum samples of Permian and Triassic age from the north-eastern Italian Alps: Palaeoenvironmental implications. *Chem. Geol.* **2007**, *245*, 275–284. [[CrossRef](#)]
46. Lloyd, R.M. Oxygen-18 composition of oceanic sulfate. *Science* **1967**, *156*, 1228–1231. [[CrossRef](#)] [[PubMed](#)]
47. Balci, N.; Shanks, W.C., III; Mayer, B.; Mandernack, K.W. Oxygen and sulfur isotope systematics of sulfate produced by bacterial and abiotic oxidation of pyrite. *Geochim. Cosmochim. Acta* **2007**, *71*, 3796–3811. [[CrossRef](#)]
48. Mangalo, M.; Meckenstock, R.U.; Stichler, W.; Einsiedl, F. Stable isotope fractionation during bacterial sulfate reduction is controlled by reoxidation of intermediates. *Geochim. Cosmochim. Acta* **2007**, *71*, 4161–4171. [[CrossRef](#)]
49. Yao, W.; Paytan, A.; Wortmann, U.G. Effects of a transient marine sulfur reservoir on seawater  $\delta^{18}\text{O}_{\text{SO}_4}$  during the Paleocene-Eocene Thermal Maximum. *Geochim. Cosmochim. Acta* **2020**, *269*, 257–269. [[CrossRef](#)]
50. Turchyn, A.V.; Schrag, D.P. Cenozoic evolution of the sulfur cycle: Insight from oxygen isotopes in marine sulfate. *Earth Planet Sci. Lett.* **2006**, *241*, 763–779. [[CrossRef](#)]
51. Turchyn, A.V.; Brüchert, V.; Lyons, T.W.; Engel, G.S.; Balci, N.; Schrag, D.P.; Brunner, B. Kinetic oxygen isotope effects during dissimilatory sulfate reduction: A combined theoretical and experimental approach. *Geochim. Cosmochim. Acta* **2010**, *74*, 2011–2024. [[CrossRef](#)]
52. Chen, G.; Yin, H.; Chu, Y. Characteristics and geological significance of organic matter contained in Tertiary ore deposits in Lanping-Simao Basin, west Yunnan. *Miner. Depos.* **1996**, *15*, 374–380. (In Chinese)
53. Lu, F.H.; Meyers, W.J.; Schoonen, M.A. S and O (SO<sub>4</sub>) isotopes, simultaneous modeling, and environmental significance of the Nijar Messinian gypsum, Spain. *Geochim. Cosmochim. Acta* **2001**, *65*, 3081–3092. [[CrossRef](#)]
54. Kristall, B.; Jacobson, A.D.; Sageman, B.B.; Hurtgen, M.T. Coupled strontium-sulfur cycle modeling and the Early Cretaceous sulfur isotope record. *Palaeogeogr. Palaeoclimatol. Palaeoecol.* **2018**, *496*, 305–322. [[CrossRef](#)]
55. Longinelli, A. Isotope geochemistry of some Messinian evaporates: Palaeoenvironmental implications. *Palaeogeogr. Palaeoclimatol. Palaeoecol.* **1979**, *29*, 95–123. [[CrossRef](#)]
56. Fontes, J.C.; Pierre, C. Oxygen 18 changes in dissolved sulphate during sea water evaporation in saline ponds. In Proceedings of the 10th International Congress on Sedimentology, Jerusalem, Israel, 9–14 July 1978; International Accounting Standards (IASs): London, UK, 1978; pp. 215–216.